J. Chem. Sci. (2020)132:13
https://doi.org/10.1007/s12039-019-1716-4

REGULAR ARTICLE

Synergistic cobalt–nickel co-catalyst for enhanced visible light-induced photocatalytic water oxidation

PEGAH NAZARI, OMID NOURI and SHAHRBANOO RAHMAN SETAYESH*
Department of Chemistry, Sharif University of Technology, Azadi Avenue, PO Box 11155-3516, Tehran, Iran
E-mail: setayesh@sharif.edu; nazari_pegah@ch.sharif.edu; omid.nouri@ch.sharif.ir

MS received 10 July 2019; revised 31 August 2019; accepted 5 September 2019

Abstract. The loading of co-catalyst is an efficient way to increase the activity of synthesized carbon-based photocatalysts in the energy and environmental applications. Herein, Co and Ni decorated on g-C_3N_4 was synthesized as a visible light active photocatalyst and characterized with XRD, FT-IR, BET, DRS, TGA, FE-SEM, EDX, and EIS techniques. From the characterization results, it was demonstrated that cobalt and nickel which were present in the structure of the nanocatalyst, were in the metallic form. The decoration of Ni and Co reduced bandgap energy of g-C_3N_4 and made the synthesized nanocomposite active under visible light. The operating condition of O_2 photocatalytic generation was optimized (193.75 μmol L^{-1} O_2 productions using 0.2 g Co2Ni1/g-C_3N_4/rGO at 7 h without sacrificial reagents). The effect of sacrificial reagents ($Fe(NO_3)_3$, $AgNO_3$, and methanol) was investigated and $Fe(NO_3)_3$ showed the best results during water oxidation. The kinetics study indicates that the presence of cocatalysts could be helpful in reducing the apparent activation energy about 3.5 times. The photocatalyst represented acceptable stability (2% Ni and 3% Co leaching) and reusability up to six cycles. According to the obtained results, we can introduce Co2Ni1/g-C_3N_4/rGO as a potential powerful photocatalyst for water oxidation reaction under visible light.

Keywords. Water oxidation; g-C_3N_4; visible light photocatalyst; co-catalyst.

1. Introduction

The energy shortage and environmental concerns have attracted great attention in scientific researches and industrial projects. Photocatalytic water splitting and pollutants degradation are green and eco-friendly promising ways to solve these global issues. Finding efficient and highly active semiconductor photocatalyst which is active in visible light and has acceptable stability during the photocatalytic processes is a new challenge in developing solar energy technologies.[1] In spite of huge researches in this field, synthesized photocatalysts with high efficiency in visible light and good stability are a limited number.[2]

Two-dimensional (2-D) metal-free materials, such as graphene, carbon nitride, and boron carbide are layered materials with large surface area and high electrical conductivity. These materials are one of the best candidates for applying as the active species in energy storage and environmental treatment technologies.[3] Graphitic carbon nitride is a stable allotrope in the ambient condition with good photocatalytic properties under visible light. Pristine g-C_3N_4 could be synthesized from low-cost nitrogen-rich precursors (melamine, urea, and cyanamide) *via* thermal polymerization in one facile step. Its optical properties ($\sim$2.7 eV bandgap and adequate overpotential for water splitting), low cost, and stability make g-C_3N_4 an ideal choice for photocatalytic reactions in energy storage and environmental remediation fields. However, g-C_3N_4 suffers from fast electron-hole recombination which leads to low efficiency in photocatalytic performances.[4] Hence, preparation g-C_3N_4-based photocatalyst to improve the charge carriers separation is one of the most important research directions in environmental and energy applications.[5] The rational design of novel heterostructures can suppress the electron-hole recombination and develop g-C_3N_4 photocatalytic activity *via* synergistic effect

*For correspondence

Electronic supplementary material: The online version of this article (https://doi.org/10.1007/s12039-019-1716-4) contains supplementary material, which is available to authorized users.

Published online: 19 December 2019

between the active species and added components. Z-scheme heterojunctions,[6] p-n heterojunctions,[7] nano-architectures,[8] and proper co-catalysts loading are some examples of the attempts to reach an ideal photocatalyst for desired applications.[9] Among these various efforts to modify g-C_3N_4, loading co-catalysts is a promising approach to raise the photocatalytic O_2 evolution.[10,11] The presence of co-catalysts causes charge separation enhancement, charge transfer acceleration, surface reaction speed-up, and back reaction suppress. Metal oxides such as IrO_2 and RuO_2 are the most popular and effective catalysts for water oxidation in acidic and basic conditions.[12] Though, the high cost and low abundance make them the expensive candidates for these kinds of reactions which are not economically viable.[13] Exploring new co-catalysts with reasonable cost, high abundance, and durability become the most attractive topics in scientific researches in oxygen evolution processes. NiO, $Ni(OH)_2$, $Ni(dmgH)_2$, and layered hydroxides are reported as the alternative co-catalysts for water oxidation reactions. Ni-based co-catalysts which decorated on g-C_3N_4 photocatalysts have moderate activity through O_2 evolution due to their low stability and conductivity.[14] Co-based catalysts present better performance towards photocatalytic water oxidation due to their interesting properties.[15] Decorated cobalt species on the surface of g-C_3N_4 provide active sites for surface oxygen evolution reaction. Moreover, coordination of Co to g-C_3N_4 and Co–N bond-forming may make available active sites for photocatalytic activities. Co-Ni-S based co-catalysts had been prepared for the electrocatalytic purpose.[16,17] It seems that the synergistic effect between Ni and Co can help to improve their photocatalytic performance.

In this work, the novel Co/g-C_3N_4/rGO, and Ni/g-C_3N_4/rGO, and CoNi/g-C_3N_4/rGO (with Co and Ni in different ratios) photocatalysts were synthesized and characterized with various techniques. The photocatalytic water oxidation as the performance of the photocatalyst was evaluated. The effect of operating parameters on the catalyst activity was studied and the photocatalytic mechanism of water oxidation was discussed. The stability and reusability of the photocatalyst as the important factors in its efficiency were studied.

2. Experimental

2.1 *Materials*

Graphite powder, sulfuric acid (95–98%), sodium nitrate, potassium permanganate, hydrochloric acid, melamine, hydrogen peroxide (30%), cobalt nitrate hexahydrate, nickel nitrate hexahydrate, polyvinylpyrrolidone (PVP) (MW = 58000), sodium hydroxide, ethanol, silver nitrate, iron nitrate nonahydrate, and methanol were all purchased from Merck (Darmstadt, Germany). All the materials were utilized without any other purification.

2.2 *Catalyst preparation*

2.2a *Graphene oxide (GO) synthesis*: The modified Hummers method was used for the preparation of graphene oxide.[18] 1.0 g of graphite powder was mixed with 0.5 g of sodium nitrate and 23 mL of sulfuric acid was added to the mixture. The resulted mixture was stirred using magnetic stirrer for 1 h. In the next step, 3.0 g of potassium permanganate was added gradually while the temperature was keeping under 293 K. After stirring the solution 12 h at 308 K, 500 mL deionized water (DI-water) was added to it. In order to complete the reaction, 5 mL hydrogen peroxide 30% was poured to the solution. The obtained mixture was rinsed with washed with 5% HCl solution and DI-water, respectively. After filtration, the precipitates were dried at 353 K under the vacuum for 24 h.

2.2b *Graphitic carbon nitride (g-C_3N_4) synthesis*: 10.0 g of melamine powder in a crucible was put in the furnace with proper temperature program. The temperature was raised from 298 K to 673 K with the rate of $\sim$2 K min^{-1}. The temperature was kept at 673 K for 30 min and at the next step, it increased to 723 K with the rate of 2.5 K min^{-1}. The temperature was kept at 723 K for 45 min and then was raised to 773 K with a rate of 2.5 K min^{-1}. At the final stage, the powder was kept at 773 K for 30 min. The obtained yellow powder was found to be g-C_3N_4.

2.2c *Metal/g-C_3N_4/rGO synthesis*: 250 mg of graphene oxide (GO) was added to 75 mL DI-water and kept in an ultrasound bath for 2 h. 0.05 mol cobalt nitrate hexahydrate and 0.05 mol nickel nitrate hexahydrate (for the other catalysts, the mole ratio of metal nitrates was varied) were added to the solution. 0.5 g of polyvinylpyrrolidone as a template was solved in 10 mL of DI-water and was added to GO and metal nitrate solution. The resulted solution was stirred for 6 h. The other solution containing 450 mg sodium hydroxide in 10 mL DI-water was poured to the first solution and stirred for 30 min. The obtained mixture was added to Teflon lined autoclave and heated for 24 h at 453 K. After cooling to room temperature, the precipitate was dried at 323 K to build the proper structure. Some water was added to make a pasty mixture. 250 mg melamine in 20 mL DI-water was added to the mixture under stirring and heating until participates completely dried. For the catalyst calcination, the

temperature was raised to 723 K with the heat rate of 5 K min^{-1} and the powder was heated at 723 K for 4 h.

2.3 *Characterization*

The structure and crystallinity of samples were recognized by X-ray powder diffraction (XRD) using X'Pert PRO MPD PANalytical (Almelo, Netherlands) with Cu Kα radiation, 40 kV and 40 mA. Fourier transform infrared (FT-IR) spectra were recorded by an ABB-Bomem model NB (Quebec, Canada). The surface area and porosity of synthesized catalysts were identified from Brunauer–Emmett–Teller (BET) technique by N_2 adsorption and desorption measurements at 77 K in a Belsorp mini II (Osaka, Japan). The optical properties of samples were measured by UV-vis diffuse reflection spectroscopy (DRS) with Avantes spectrometer Avaspec-2048-TEC model and AvaLamp DH-S Setup (Apeldoorn, Netherlands). Thermogravimetric analysis (TGA) was carried out on a TGA/DSC thermal analyzer of Mettler Toledo (Ohio, USA) under a nitrogen atmosphere with a heating rate of 5 °C min^{-1}. The morphological properties of the synthesized catalysts were evaluated by field emission scanning electron microscopy (FE-SEM) and EDX using TeScan-Mira (III) microscope (Brno, Czech Republic). Electrochemical impedance spectroscopy (EIS) measurements were carried out by the potentiostat/galvanostat EG&G model 273A (Maryland, USA).

2.4 *Experimental procedure and analytical methods*

The experiments were carried out in a PVC box which was equipped with 4 LED (nominal power: 6 W) lamps with ~450 nm emission wavelength as a source of visible light. To control the reaction temperature, a water bath connected to a thermostat was used. Four fans for air conditioning of the box and keeping the temperature about the room temperature (298 K) were utilized. A 250 mL Pyrex reactor for performing the reactions was used. For a typical photocatalytic reaction, 200 mL DI-water and 0.1 g of photocatalyst were poured to the reactor. The dissolved oxygen was removed from the solution by Ar gas purging for 30 min. After deoxygenation procedure, the gas inlet was blocked using parafilm and the solution was irradiated with visible light. The amount of generated O_2 was measured by a Lutron DO5510 oxygen meter (New Taipei City, Taiwan).

To evaluate the influence of sacrificial agents, the proper sacrificed agent was added to the solution at the beginning of the experiment.

The kinetics study was performed at different temperatures (288, 298, 308, and 318 K) with g-C_3N_4 and Co_2Ni1/g-C_3N_4/rGO as photocatalysts under visible light.

The leaching of cobalt and nickel were measured by ICP-OES Varian model 730-ES (California, USA).

3. Results and Discussion

3.1 *Characterization*

The crystallinity and crystal structure of the synthesized catalysts were analyzed by XRD. The XRD patterns of catalysts are presented in Figure 1. The peaks at 2θ = 15.23°, 21.54°, and 27.92° in XRD pattern of g-C_3N_4/rGO can be assigned to the layer structure of the synthesized compound. The peak located at 21.54° was assigned to (002) the plane of graphene oxide which is reduced to rGO. Two peaks at 15.23° and 27.92° are related to (100) and (002) crystal planes of graphitic carbon nitride which has a porous structure and conjugated aromatic system (JCPDS No. 87-1526).[19] In the XRD pattern of Co/g-C_3N_4/rGO, the intensity of the characteristic peaks of g-C_3N_4 was diminished which can be due to the prevention of melamine thermal polymerization to graphitic carbon nitride by cobalt.[14] The same results were observed in the pattern of Ni/g-C_3N_4/rGO. In the Co2Ni1/g-C_3N_4/rGO XRD pattern, the presence of Co and Ni caused a decrease in g-C_3N_4 characteristic peaks due to inhibition of the melamine thermal polymerization. The peaks of Co and Ni crystalline structures did not observe in diffractogram, owing to the low amount of them. In all patterns of samples, the peaks around 15° and 28° are related to the structure of g-C_3N_4. The mean values for particle sizes of synthesized catalysts are presented in Table 1. The Scherrer's equation was applied for calculating the particle sizes.[20]

Figure 2 presents the FT-IR spectra of the synthesized nanocomposites. The peaks around 1000, 1200, and 1600–1700 cm^{-1} which are related to C-O-C, C-O, and COOH vibrations, respectively, did not appear in the spectrum of reduced graphene oxide. This means that the reduction of graphene oxide has been carried out successfully.[19] In the spectrum of g-C_3N_4, the peak at 807 cm^{-1} demonstrated the

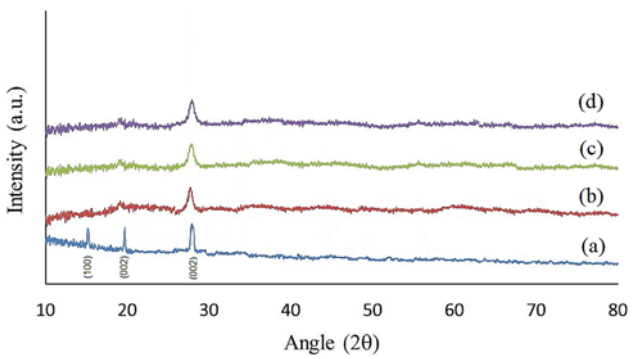

Figure 1. XRD patterns of (a) g-C_3N_4/rGO, (b) Co/g-C_3N_4/rGO, (c) Ni/g-C_3N_4/rGO, (d) Co2Ni1/g-C_3N_4/rGO.

existence of tri-*s*-triazine or cyamelurine. The presence of peaks at 1242, 1322, 1412, 1563, and 1634 cm^{-1} are attributed to C-N and C=N stretching vibration in g-C_3N_4 heterocycles.[21] The peaks at 810 and 1200–1650 cm^{-1} are related to stretching vibration modes of heterocycles of graphitic carbon nitride in Co/g-C_3N_4/rGO. The obtained peaks at 3130 and 3150 cm^{-1} can be due to primary and secondary amine functional groups and N-H vibration. For Ni/g-C_3N_4/rGO the addition of nickel to g-C_3N_4/rGO does not cause any significant change in the spectrum. In the simultaneous presence of cobalt and nickel in the synthesized nanocomposite, the intensity of the characteristic peaks of g-C_3N_4 decreases owing to the deamination accelerating by metals.[22]

In heterogeneous catalyst, the catalytic reactions occur on the surface of the catalyst. Therefore, the knowledge about the surface and texture of the active species is crucial. To achieve this goal the N_2 adsorption and desorption isotherms were used. The surface area, mean pore diameter, and total pore volume of Co2Ni1/g-C_3N_4/rGO are 32.96 m^2 g^{-1}, 4.17 nm, and 0.19 mL g^{-1}, respectively. The adsorption isotherm of the catalyst as illustrated in Figure S2 (Supplementary Information) is of type II in IUPAC classification, which can be attributed to the nonporous materials or macroporous materials.[23]

The optical properties of catalysts were studied by UV-vis diffuse reflection spectra (DRS). The impact of metal cocatalyst usage on the electronic properties of g-C_3N_4 was shown in Figure 3. The incorporation of Ni and Co decreased the bandgap of the nanocomposite gradually and showed extended visible-light adsorption (Table 2). Especially, in Co2Ni1/g-C_3N_4/rGO the reduction of the bandgap is considerable, which may be due to the charge transfer like the ligand to the metal charge transition in the system.[24]

The thermal stability of the catalyst was measured by TGA under an air atmosphere from 25 to 1200 °C (Figure 4). At the first step, the water molecules were evaporated. The decomposition of PVP started at the next step, from 197.95 to 314.14 °C. The final step of the catalyst decomposition initiated from 450 °C and completed at 695.45 °C, which is due to the g-C_3N_4 decomposition. The initial temperature of g-C_3N_4 decomposition is lower than the pure g-C_3N_4 which is due to the catalytic effect of metals for enhancing the support oxidation.[25]

The morphology and texture of as-prepared catalysts were evaluated by FE-SEM analysis. Figure 5 illustrates the FE-SEM image of pure g-C_3N_4, g-C_3N_4/rGO, and Co2Ni1/g-C_3N_4/rGO with the same magnification. The layer structure of g-C_3N_4 and g-C_3N_4/rGO is shown in the images. It was seen that the

Table 1. Particle size of the synthesized photocatalysts from XRD.

Catalyst	Particle size (nm)
g-C_3N_4	48.82
Ni/g-C_3N_4/rGO	13.64
Co/g-C_3N_4/rGO	13.92
Co2Ni1/g-C_3N_4/rGO	14.11

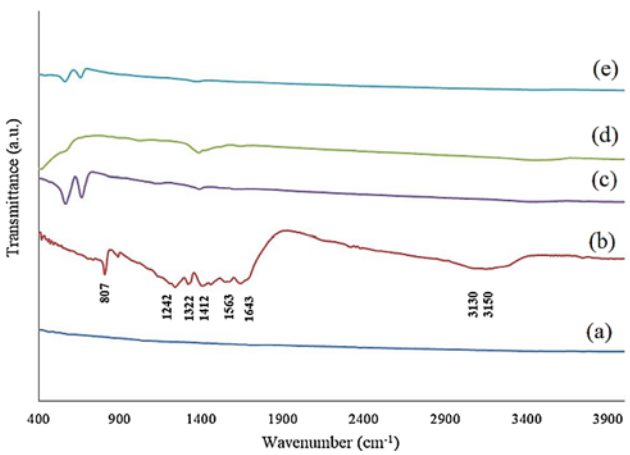

Figure 2. FT-IR spectra of (a) rGO, (b) g-C_3N_4, (c) Co/g-C_3N_4/rGO, (d) Ni/g-C_3N_4/rGO, (e) Co2Ni1/g-C_3N_4/rGO.

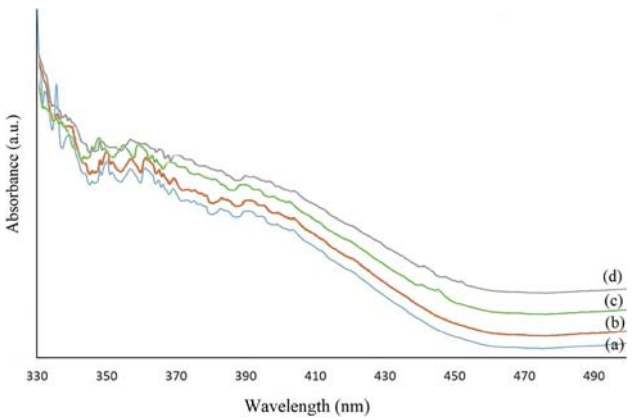

Figure 3. DRS spectra of (a) g-C_3N_4, (b) Ni/g-C_3N_4/rGO, (c) Co/g-C_3N_4/rGO, (d) Co2Ni1/g-C_3N_4/rGO.

Table 2. Band gap of the synthesized photocatalysts.

Catalyst	Particle size (nm)
g-C_3N_4	2.75
Ni/g-C_3N_4/rGO	2.71
Co/g-C_3N_4/rGO	2.61
Co2Ni1/g-C_3N_4/rGO	2.30

Co2Ni1/g-C_3N_4/rGO has a hexagonal structure which may be the result of the coordination of cobalt to g-C_3N_4. The coordination of Co^{2+} and Ni^{2+} to nitrogen of g-C_3N_4 (electron donor part of g-C_3N_4) has been illustrated in Figure 5 (d). The elemental and chemical analysis of the synthesized samples was performed by the EDX technique (Figure S3, Supplementary Information). In the g-C_3N_4 EDX spectrum, there are only carbon and nitrogen peaks, while the peak of oxygen attributed to rGO appeared in the g-C_3N_4/rGO spectrum. The presence of the Ni and Co in the EDX spectrum of Co2Ni1/g-C_3N_4/rGO confirms the elemental structure of the catalyst.

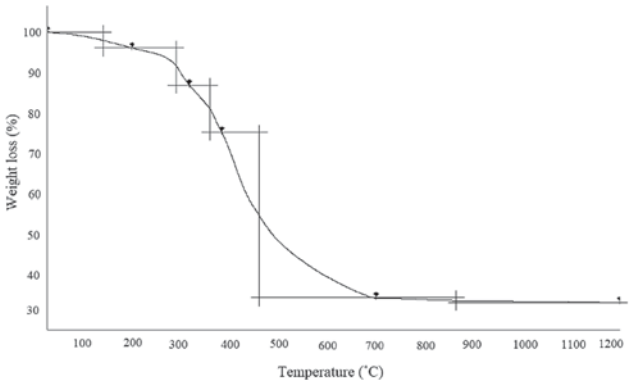

Figure 4. TGA curve of Co2Ni1/g-C_3N_4/rGO.

3.2 *Impact of operational parameters*

To evaluate the effective parameters on water oxidation through the photocatalytic reaction, the influence of reaction time, photocatalyst, and the amount of the photocatalyst were studied.

3.2a *The effect of reaction time*: The evaluation of the reaction time parameter on the photocatalytic oxygen evolution was performed (Figure 6 (a)). It was observed that the amount of produced oxygen reached 112.5 μmol L^{-1} after 7 h while the oxygen production increased by only 9.5 μmol L^{-1} in the next 9 h. 7 h was selected as the optimum reaction time for further experiments.

3.2b *The effect of cobalt and nickel co-catalysts*: The photocatalytic activities of synthesized catalysts were studied *via* measuring the oxygen evolution in the aqueous solution under visible light irradiation. Two experiments, with no irradiation or photocatalyst, were performed to identify the

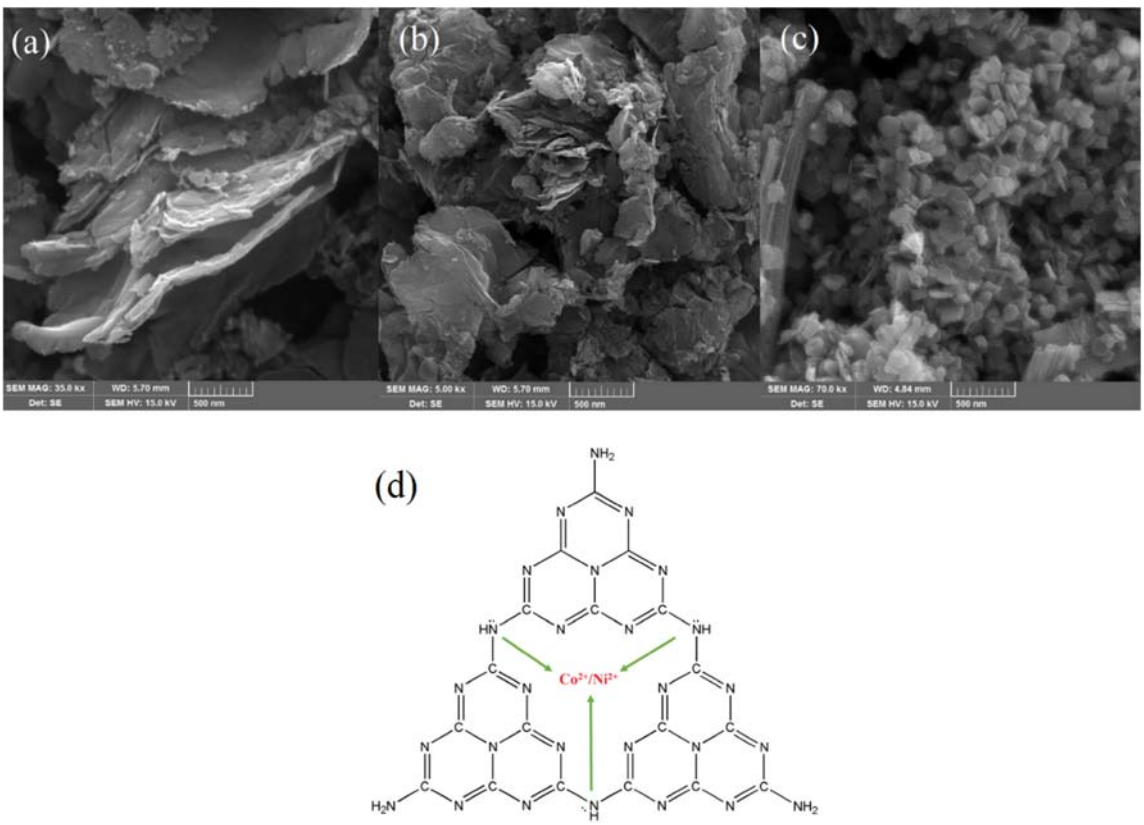

Figure 5. FE-SEM images of (a) g-C_3N_4, (b) g-C_3N_4/rGO, (c) Co2Ni1/g-C_3N_4/rGO, (d) schematic illustration of Co and Ni coordination to g-C_3N_4.

portion of the photocatalytic reaction in O_2 evolution. It was observed that no remarkable O_2 generation was detected. In the case of pure g-C_3N_4 usage as a photocatalyst, the amount of oxygen is very low attributed to quick recombination of electrons and holes in the conduction band (CB) and the valence band (VB), respectively. This rapid phenomenon in g-C_3N_4 makes it an inactive photocatalyst for O_2 evolution under visible light. The incorporation of metals (Co and Ni) into the photocatalyst can improve the performance of synthesized g-C_3N_4 by deceleration of electron-hole recombination procedure. Introducing metals (Co and Ni) as cocatalysts to g-C_3N_4 structure accelerated the rate of charge carriers transition and raised the O_2 evolution by water oxidation. Meanwhile, nickel has the hole capture property moderately and reduced the photocatalytic performance of the synthesized nanocomposites.[26] The Ni-photocatalysts showed weaker results in comparison with Co-containing photocatalysts (78.12 μmol L^{-1} for Ni/g-C_3N_4/rGO vs. 90.62 μmol L^{-1} for Co/g-C_3N_4/rGO). The best result was achieved by the utilization of Co2Ni1/g-C_3N_4/rGO (184.37 μmol L^{-1}), which is in accordance with the mentioned metals (Co and Ni) characters. The results are shown in Figure 6 (b). The electron transfer procedure in the photocatalyst was studied by EIS measurement. The Nyquist plots of g-C_3N_4 and Co2Ni1/g-C_3N_4/rGO are presented in Figure 7. The smaller diameter of the semicircle in the Nyquist plot indicates that the smaller residence of electron transfer, which would boost the electron transition efficiency in the synthesized photocatalyst for the water oxidation reaction.[26] The diameter of the semicircle in Nyquist plot of Co2Ni1/g-C_3N_4/rGO was smaller than for g-C_3N_4, which confirmed that the electron-hole pair separation was more efficient in the Co2Ni1/g-C_3N_4/rGO in comparison with pure g-C_3N_4 and the recombination of electron-hole pair was decreased.

3.2c *The effect of catalyst weight*: To study the impact of the catalyst weight, a set of experiments with various amount of the catalyst were set (Figure 6 (c)). The increase of photocatalyst from 0.05 to 0.20 g enhanced the O_2 evolution from 156.25 to 193.75 μmol L^{-1}. It can be owing to the more available active sites for photocatalytic water oxidation. Further adding the catalyst to 0.25 g reduced the oxygen evolution to 177.50 μmol L^{-1}. It may due to the turbidity of the solution which prevented from reaching the light to the photocatalytic active species.[27] 0.20 g Co2Ni1/g-C_3N_4/rGO was selected as the optimum amount of photocatalyst for this system.

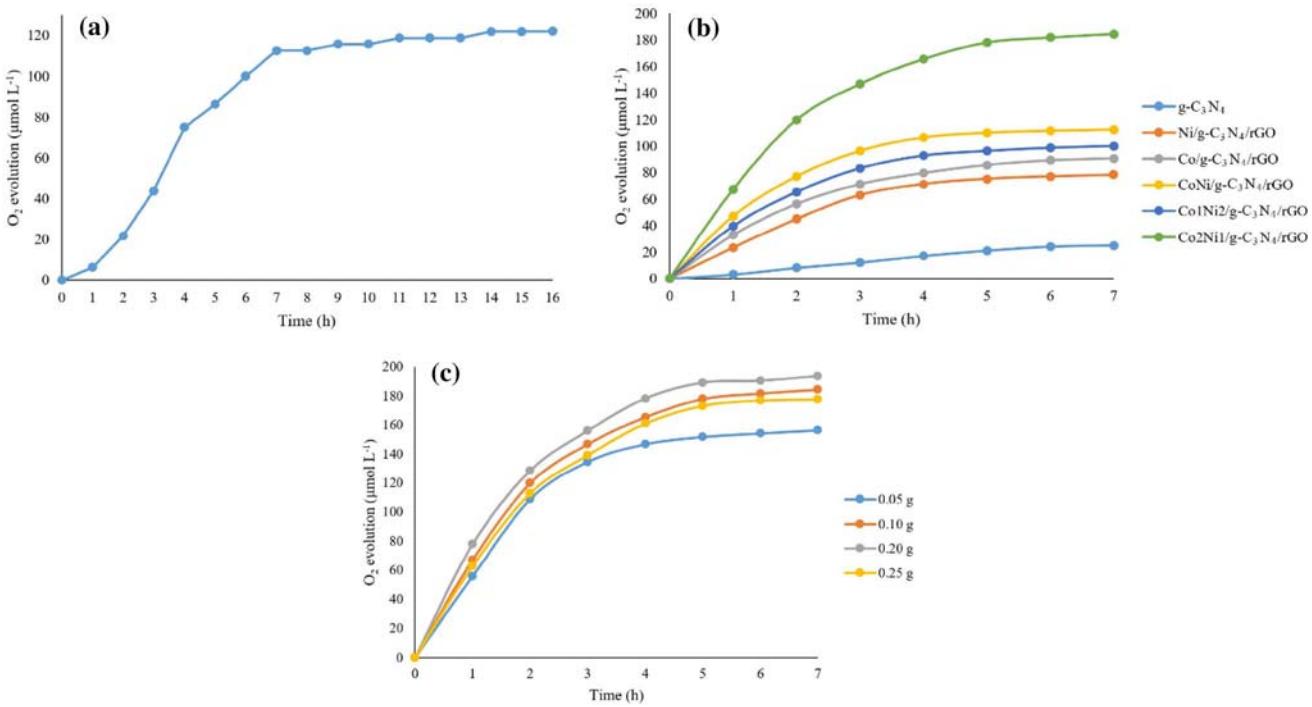

Figure 6. (a) Effect of reaction time (0.10 g of CoNi/g-C_3N_4/rGO), (b) effect of co-catalysts (0.10 g of photocatalyst at 7 h), (c) effect of catalyst weight (Co2Ni1/g-C_3N_4/rGO at 7 h).

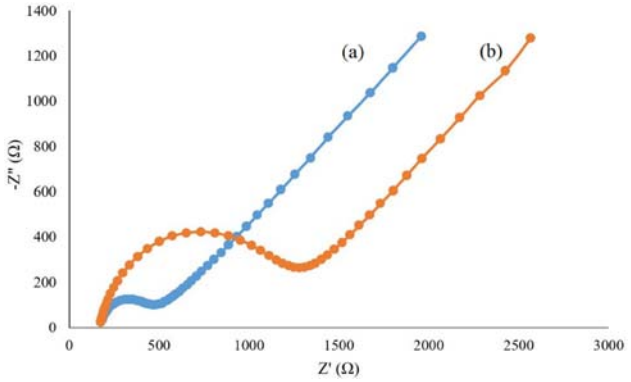

Figure 7. Electrochemical impedance spectroscopy (EIS) curves of (a) g-C_3N_4, (b) Co2Ni1/g-C_3N_4/rGO.

The turnover number (TON) and turnover frequency (TOF) values of the photocatalyst were calculated using equations 1 and 2.

$$\text{Turnover number (TON)} = \text{Moles of formed product/Moles of catalyst} \quad (1)$$

$$\text{Turnover frequency (TOF)} = \text{Turnover number/Reaction time} \quad (2)$$

Calculating the apparent quantum efficiency (QE), which is an important parameter in photocatalytic reactions, can provide valuable data about the efficiency of the photocatalysis procedure. QE was measured by putting 4 monochromatic LED sources (6 mW power and 1.359×10^{19} photon per second) in 1 cm distance from the reactor and QE was calculated by the following equation:

$$\text{QE}\ (\%) = (\text{Number of } O_2 \text{ molecules} / \text{Number of incident photons}) \times 100 \quad (3)$$

The results of TON, TOF, and QE have been reported in Table 3.

3.3 *Sacrificial reagents in photocatalytic water oxidation*

During the light irradiation with the energy equals to or larger than the semiconductor bandgap, the excited electrons in the CB have the ability to reduce the H_2O to H_2. Simultaneously, the holes in the VB can oxidize H_2O to O_2. Sacrificial reagents (SRs) are widely utilized in the photocatalytic water splitting systems to manage the reaction through the desired pathway and improve quantum efficiency. $AgNO_3$ and $Fe(NO_3)_3$ are two electron scavenger (ES) compounds which can direct the reaction to oxygen evolution. The application of these two ES compounds caused the enhancement in O_2 formation at the first four hours of the reaction in comparison with the absence of SRs (Figure 8). The redox potentials for Ag^+/Ag and Fe^{3+}/Fe^{2+} are 0.779 and 0.77 V vs NHE, respectively, which are larger than that of H^+/H_2. It can be indicated that Ag^+ and Fe^{3+} will gain the electrons and inhibit from reacting with H^+ and H_2 generation (Eq. 4 and 5).[28]

$$4Ag^+ + 2H_2O \xrightarrow{h\nu} O_2 + 4H^+ + 4Ag \downarrow \quad (4)$$

$$4Fe^{3+} + 2H_2O \xrightarrow{h\nu} O_2 + 4H^+ + 4Fe^{2+} \quad (5)$$

It has been observed that the amount of oxygen formation in the presence of $AgNO_3$ was lower than $Fe(NO_3)_3$. It was expected that the metallic silver production can promote the reaction (4) and increase the O_2 formation however the results were something else and the amount of oxygen evolution in the presence of $Fe(NO_3)_3$ was slightly larger. It may be due to the precipitation of metallic Ag on the surface of catalyst or reaction container and inhibition from the desired photocatalytic reactions.

To ensure the reaction pathway, methanol as an electron donor (ED) compound was used. The obtained results indicated that when methanol was used in the reaction, O_2 generation was stopped and the electrons were guided to the reaction (6) to produce H_2.[29]

$$CH_3OH + H_2O \xrightarrow{h\nu} CO_2 + 3H_2 \quad (6)$$

3.4 *Kinetics study*

The Arrhenius plots (ln r vs. T^{-1}) for two situations (g-C_3N_4 and Co2Ni1/g-C_3N_4/rGO as photocatalysts) were drawn (Figure 9). The apparent activation energies for these two operational conditions were extracted from the slope of the plots.

The activation energy was calculated from the Arrhenius equation as follows:

$$Ea = -R[d \ln r/d(1/T)] \quad (7)$$

To further find out the impact of cocatalyst in the kinetics of photocatalytic water oxidation under visible light, kinetics study of two systems (in the presence and absence of cocatalyst) was carried out. The apparent activation energy (Ea) of g-C_3N_4 and Co2Ni1/g-C_3N_4/rGO are 16.13 and 4.62 kJ mol^{-1},

Table 3. Performance of catalysts in photocatalytic water oxidation (0.2 g catalyst at 7 h without sacrificial reagents).

Catalyst	TON × 10^1	TOF × 10^2 (h^{-1})	QE (%)
g-C_3N_4	0.79	1.13	0.12
Ni/g-C_3N_4/rGO	2.02	2.88	0.30
Co/g-C_3N_4/rGO	2.31	3.30	0.35
CoNi/g-C_3N_4/rGO	2.82	4.03	0.43
Co1Ni2/g-C_3N_4/rGO	2.53	3.61	0.38
Co2Ni1/g-C_3N_4/rGO	4.48	6.40	0.68

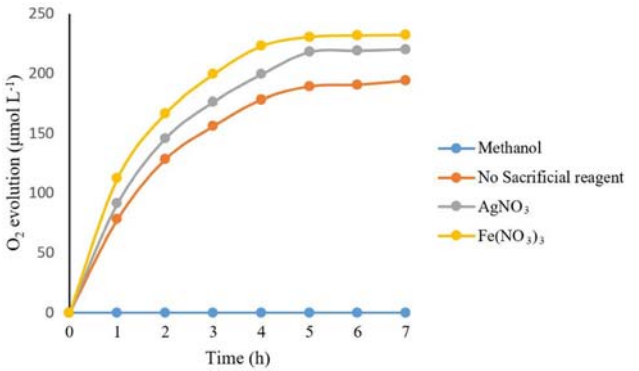

Figure 8. Effect of sacrificial reagents on O_2 evolution (1.75 g $Fe(NO_3)_3$ or 10 mL methanol or 2.0 g $AgNO_3$) 0.20 g Co2Ni1/g-C_3N_4/rGO at 7 h.

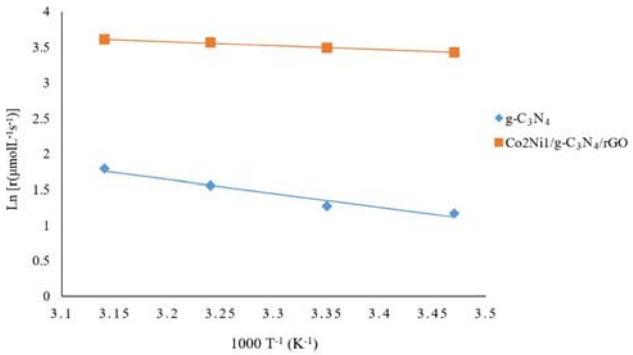

Figure 9. Arrhenius plot of O_2 evolution rate ln(r) vs. 1/T over g-C_3N_4 and Co2Ni1/g-C_3N_4/rGO.

respectively. The amount of activation energy in the absence of cocatalyst is near to the values for thermal reaction, which is relatively high for photocatalytic reactions. The usage of cocatalyst caused a reduction of about 3.5 times in the apparent activation energy of the water oxidation reaction.[30] The schematic role of cocatalysts in a decrease of the activation energy is illustrated in Figure S5 (Supplementary Information).

3.5 *Leaching evaluation*

To find out the stability of the photocatalyst against leaching into the experiment solution, the amount of dissolved metal (Co and Ni) was measured using ICP technique. An experiment at the operational condition: 200 mL DI-water, 0.2 g Co2Ni1/g-C_3N_4/rGO as the photocatalyst, at 7 h photocatalytic reaction. The amount of leached metals from as-synthesized photocatalyst was measured and it was shown that only 2 and 3% of Ni and Co were dissolved, respectively. According to the results, the metals were immobilized successfully on g-C_3N_4/rGO and the probable homogeneous photocatalytic reaction was insignificant. It can be inferred that the heterogeneous photocatalytic reaction has the main role in water oxidation in this system.

3.6 *Catalyst reusability and tracing the fate of photocatalyst*

The stability of the heterogeneous catalyst is an important issue in catalytic applications. To evaluate the stability of the as-synthesized catalyst, Co2Ni1/g-C_3N_4/rGO was recycled for other five more cycles. It was seen that there is no considerable loss in the catalytic performance of the nanocomposite. The presented results in Figure 10 indicate the good stability of Co2Ni1/g-C_3N_4/rGO in the experimental conditions and can utilize several times which is the characteristic

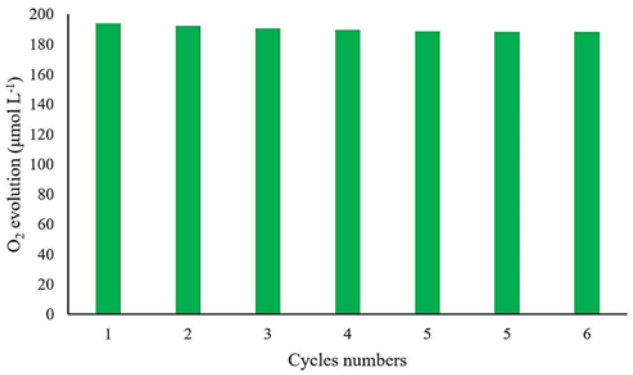

Figure 10. Reusability of catalyst for O_2 evolution (0.2 g Co2Ni1/g-C_3N_4/rGO at 7 h).

property of the applicable heterogeneous photocatalysts.

The fate of the photocatalyst was investigated by XRD technique (Figure S6, Supplementary Information). The XRD patterns of Co2Ni1/g-C_3N_4/rGO before and after water oxidation reaction did not change significantly and it can be concluded that the structural rearrangement had not happened.

4. Conclusions

Cobalt and nickel were loaded on the g-C_3N_4 as the co-catalysts to increase the photocatalytic oxygen evolution under visible light irradiation. The results of characterization techniques indicated that metallic cobalt and nickel are decorated on the layer structure of g-C_3N_4/rGO. The metallic co-catalysts reduced the bandgap of nanocatalyst and showed extended visible-light adsorption. The impact of the molar ratio of metals was investigated and it was observed that the molar ratio of 2:1 of Co: Ni presented the best result towards oxygen evolution reaction. The usage of sacrificial reagents improved the formation of oxygen and iron nitrate revealed the best result (232.19 μmol L^{-1}). The loading of cocatalyst can improve the apparent activation energy barrier about 3.5 times for photocatalytic water oxidation reaction. The high stability of photocatalyst was proved by leaching test (2% Ni and 3% Co leached). The synthesized photocatalyst showed acceptable recyclability up to six cycles. It can be concluded that Co2Ni1/g-C_3N_4/rGO can be considered as a promising photocatalyst for O_2 evolution under visible light.

Supplementary Information (SI)

Figures S1-S6 are available at www.ias.ac.in/chemsci.

Acknowledgements

The authors are thankful to the chemistry department of Sharif University of Technology for financial support.

Conflict of interest The authors declare that they have no conflict of interest.

References

1. Kudo A, Yoshino S, Tsuchiya T, Udagawa Y, Takahashi Y, Yamaguchi M, Ogasawara I, Masumoto H and Iwase A 2019 Z-scheme photocatalyst systems employing Rh- and Ir-doped metal oxide materials for water splitting under visible light irradiation *Faraday Discuss.* **215** 313
2. Takata T and Domen K 2019 Particulate photocatalysts for water splitting: recent advances and future prospects *ACS Energy Lett.* **4** 542
3. Yan J, Wu H, Chen H, Pang L, Zhang Y, Jiang R, Li L and Liu S 2016 One-pot hydrothermal fabrication of layered β-Ni$(OH)_2$/g-C_3N_4 nanohybrids for enhanced photocatalytic water splitting *Appl. Catal. B* **194** 74
4. Wen J, Xi J, Chen X and Li X 2017 A review on g-C_3N_4-based photocatalysts *Appl. Surf. Sci.* **391** 72
5. Fu J, Yu J, Jiang C and Cheng B 2018 g-C_3N_4-based heterostructured photocatalysts *Adv. Mater. Res.* **8** 1701503
6. Xie Z, Feng Y, Wang F, Chen D, Zhang Q, Zeng Y, Lv W and Liu G 2018 Construction of carbon dots modified MoO_3/g-C_3N_4 Z-scheme photocatalyst with enhanced visible-light photocatalytic activity for the degradation of tetracycline *Appl. Catal. B* **229** 96
7. Liang S, Zhang D, Pu X, Yao X, Han R, Yin J and Ren X 2019 A novel Ag_2O/g-C_3N_4 p-n heterojunction photocatalysts with enhanced visible and near-infrared light activity *Sep. Purif. Technol.* **210** 786
8. Mohamed M A, Jaafar J, Zain M F M, Minggu L J, Kassim M B, Rosmi M S, Alias N H, Nor N M, Salleh W N W and Othman M H D 2018 In-depth understanding of core-shell nanoarchitecture evolution of g-C_3N_4@C, N co-doped anatase/rutile: Efficient charge separation and enhanced visible-light photocatalytic performance *Appl. Surf. Sci.* **436** 302
9. Zeng D, Zhou T, Ong W, Wu M, Duan X, Xu W, Chen Y, Zhu Y and Peng D 2019 Sub-5 nm ultra-fine FeP nanodots as efficient co-catalysts modified porous g-C_3N_4 for precious-metal-free photocatalytic hydrogen evolution under visible light *ACS Appl. Mater. Interfaces* **11** 5651
10. Tian L, Xian X, Cui X, Tang H and Yang X 2019 Fabrication of modified g-C_3N_4 nanorod/Ag_3PO_4 nanocomposites for solar-driven photocatalytic oxygen evolution from water splitting *Appl. Surf. Sci.* **430** 301
11. Tian L, Yang X, Cui X, Liu Q and Tang H 2019 Fabrication of dual direct Z-scheme g-C_3N_4/MoS_2/Ag_3PO_4 photocatalyst and its oxygen evolution performance *Appl. Surf. Sci.* **463** 9
12. Wang N and Li X 2018 Protonated carbon nitride nanosheet supported IrO_2 quantum dots for pure water splitting without sacrificial reagents *Inorg. Chem. Front.* **5** 2268
13. Zhang L, Yang C, Xie Z and Wang X 2018 Cobalt manganese spinel as an effective cocatalyst for photocatalytic water oxidation *Appl. Catal. B* **224** 886
14. Wen J, Xie J, Zhang H, Zhang A, Liu Y, Chen X and Li X 2017 Constructing multifunctional metallic Ni interface layers in the g-C_3N_4 nanosheets/amorphous NiS heterojunctions for efficient photocatalytic H_2 generation *ACS Appl. Mater. Interfaces* **9** 14031
15. Yang L, Liu J, Yang L, Zhang M, Zhu H, Wang F and Yin J 2020 Co_3O_4 imbedded g-C_3N_4 heterojunction photocatalysts for visible-light-driven hydrogen evolution *Renew. Energy* **145** 619
16. Tahir M, Mahmood N, Pan L, Huang Z, Lv Z, Zhang J, Butt F K, Shen G, Zhang X, Dou S X and Zou J 2016

Efficient water oxidation through strongly coupled graphitic C_3N_4 coated cobalt hydroxide nanowires *J. Mater. Chem. A* **4** 12940
17. Shinde D, Trizio L, Dang Z, Prato M, Gaspari R and Manna L 2017 Hollow and porous nickel cobalt perselenide nanostructured microparticles for enhanced electrocatalytic oxygen evolution *Chem. Mater.* **29** 7032
18. Shahriary L and Athawale A A 2014 Graphene oxide synthesized by using modified Hummers approach *Int. J. Renew Energy Environ. Engin*. **2** 58
19. Yuan B, Wei J, Hu T, Yao H, Jiang Z, Fang Z and Chu Z 2015 Simple synthesis of g-C_3N_4/rGO hybrid catalyst for the photocatalytic degradation of rhodamine B *Chin. J. Catal*. **36** 1009
20. Monshi A, Foroughi M R and Monshi M R 2012 Modified Scherrer equation to estimate more accurately nano-crystallite size using XRD *World J. Nano Sci. Eng.* **2** 154
21. She X, Liu L, Ji H, Mo Z, Li Y, Huang L, Du D, Xu H and Li H 2016 Template-free synthesis of 2D porous ultrathin nonmetal-dopedg-C_3N_4 nanosheets with highly efficient photocatalytic H_2 evolution from water under visible light *Appl. Catal. B* **187** 144
22. Fu Y, Zhan W, Guo Y, Guo Y, Wang Y and Lu G 2017 Highly efficient cobalt-doped carbon nitride polymers for solvent-free selective oxidation of cyclohexane *Green Energy Environ.* **2** 142
23. ALOthman Z A 2012 A review: fundamental aspects of silicate mesoporous materials *Materials* **5** 2874
24. Zhang G, Huang C and Wang X 2015 Dispersing molecular cobalt in graphitic carbon nitride frameworks for photocatalytic water oxidation *Small* **11** 1215
25. Liu H, Jin Z, Xu Z, Zhang Z and Ao D 2015 Fabrication of $ZnIn_2S_4$–g-C_3N_4 sheet-on-sheet nanocomposites for efficient visible-light photocatalytic H_2-evolution and degradation of organic pollutants *RSC Adv.* **5** 97951
26. Qi K, Xie Y, Wang R, Liu S and Zhao Z 2019 Electroless plating Ni-P cocatalyst decorated g-C_3N_4 with enhanced photocatalytic water splitting for H_2 generation *Appl. Surf. Sci.* **466** 847
27. Nonakaran B G and Yangjeh A H 2016 Ternary ZnO/AgI/Ag_2CO_3 nanocomposites: novel visible-light-driven photocatalysts with excellent activity in degradation of different water pollutants *Mater. Chem. Phys*. **184** 210
28. Liu H, Yuan J and Shangguan W 2006 Photochemical reduction and oxidation of water including sacrificial reagents and Pt/TiO_2 catalyst *Energy Fuels* **20** 2289
29. Yu J, Wang S, Cheng B, Lin Z and Huang F 2013 Noble metal-free $Ni(OH)_2$–g-C_3N_4 composite photocatalyst with enhanced visible-light photocatalytic H_2-production activity *Catal. Sci. Technol.* **3** 1782
30. Ge G, Liu M, Liu C, Zhou W, Wang D, Liu L and Ye J 2019 Ultrathin FeOOH nanosheets as an efficient cocatalyst for photocatalytic water oxidation *J. Mater. Chem. A* **7** 9222